Available online at www.sciencedirect.com
ScienceDirect
Measurement 41 (2008) 885–895
Measurement
www.elsevier.com/locate/measurement

Dimension effect on mechanical behavior of silicon micro-cantilever beams

Hsien-Kuang Liu [a,*], C.H. Pan [b], Pang-Ping Liu [a]

[a] Department of Mechanical and Computer Aided Engineering, Feng Chia University, 407 Taichung, Taiwan, ROC
[b] Institute of Precision Machinery and Manufacturing Technology, National Chin-Yi Institute of Technology, 411 Taichung, Taiwan, ROC

Received 22 September 2006; received in revised form 7 May 2007; accepted 21 December 2007
Available online 17 January 2008

Abstract

The bulk micro-machining technique is commonly applied to fabricate the silicon micro-cantilever beam. With a micro-probe and special designed fixtures a micro-force testing machine can effectively apply mechanical loading on the beams by bending. This paper is thus aimed at studying the mechanical behavior of single crystal silicon (SCS) micro-cantilever beams by the specific method. The focus is at elucidating failure mechanisms of bent beams since limited studies have been conducted concerning its impact on reliability evaluation. We have fabricated various types of samples that have different lengths and thickness. With various beams in micro-scale, not only the stress–strain relationship can be achieved, but dimension effects on flexural strength, Young's modulus, and failure strain of MEMS devices can also be precisely evaluated. In addition, locations and failure modes of bent beams are detected by SEM. Based on the microscopic analysis, failure mechanisms are determined for various beams. For reliability analysis purposes it is crucial to determine the location and cause of failure. Data on strength and failure strain as found in the study can be very important for reliability evaluation of SCS such as fatigue life. The testing method can also be easily extended to nano-scale specimens by adding a force magnification lever mechanism.

Keywords: Dimension effect; Micro-cantilever beam; Mechanical loading; Bending; Flexural strength

1. Introduction

In recent years, micro-electro-mechanical system (MEMS) structures have emerged for a wide range of applications including micro-motors, accelerometers, and biomedical devices. However, one of the major barriers in the large-scale commercialization of MEMS is the development of a detailed study of failure mechanisms under various kinds of loadings [1]. Although many MEMS devices are fabricated from silicon based materials, these micro scale silicon structures may not behave similar to bulk silicon structures. Unlike bulk mechanical properties of silicon, which have received considerable attention in the literature, there have only been limited studies of mechanical properties of silicon at the micro-scale.

It is easier to test MEMS materials in bending because many microdevices that move do so parallel

* Corresponding author.
E-mail address: hkliu@fcu.edu.tw (H.-K. Liu).

0263-2241/$ - see front matter © 2008 Elsevier Ltd. All rights reserved.
doi:10.1016/j.measurement.2007.12.007

to the substrate [2]. Jadaan et al. [3] provided a good summary of the strength of both single crystal silicon (SCS) and polysilicon. Almost half of the SCS specimens were tested by bending in the beam configuration, and the strength ranged from 0.31 to 17.5 GPa; while the strength for polysilicon is in a narrower range of 0.57–4.9 GPa. The results showed that both testing methods and brittleness of the silicon lead to the variation of strength. Wilson et al. [4] found that there is variation of bending strength of the SCS micro cantilever beam tested from front surface (3.3 GPa) and from back surface (1.0 GPa) due to anisotropic etching on the back surface. Detailed studies of the influence of chemical solution in wet etching on tensile strength of SCS were done by Taechung [5]. The SCS specimen with highest strength 1.24 GPa is etched by EDP, while the lowest strength 0.63 GPa is etched by KOH. The SCS micro cantilever beam is further set up such that the loading can be applied on the side surface [6]. The beam with fracture along (1 1 0) surface shows higher strength than the one with fracture along (1 1 1) surface. Jadaan et al. [7] indicated that the SCS elastic modulus was independent of size, while the bending strength displayed significant sensitivity to size.

Recently, Chen and Ou [8] proposed a model which can predict the strength of the same material tested by another type of structure associated with a different size, geometry, and loading situation based on a known testing result. The Weibull statistics was adopted in their work for the development of the strength conversion flow. Based on previous studies, the issue needed to be addressed here is that micro-fabricated materials have properties that are highly dependent on the fabrication route used to create them and the scale of the structures that they constitute. However, the development of both standardized test methods and material property data bases has lagged behind that of the design and simulation tools, limiting their utility. Even though moduli tests on polysilicon deposited by identical process have been done, the discrepancy in moduli values has been reported probably only due to differences in experimental technique and associated measurement error at the MEMS scale. The first step towards the solution of this dilemma is to develop standard test methods with which to characterize the mechanical properties of micro-fabricated material produced by the same processes and at the same scales as the intended application.

Therefore, a simple but useful testing methodology on MEMS structures is provided in this work. The center of the methodology is applying mechanical loads via testing micro-probe on the specimens with various dimensions by a highly precise micro-force testing apparatus. This method allows testing various specimens in a larger range of forces and displacements. The bulk micro-machining technique is adopted to fabricate the micro-cantilever beam on a silicon wafer. The mechanical loading is applied on the beam by direct contact between the probe and the free end of the beam. The proposed testing methodology can probably be expected to develop as one of the standard test methods, and not only would extend applications of SCS in MEMS devices based on the better understanding of its mechanical properties, but also strengthen design and simulation tools in MEMS.

2. Experimental

2.1. Micro-cantilever beams

The material used for micro-cantilever beams is 4 in. single crystal silicon (Si) p type (1 0 0) wafer. The direction of orientation flat is [1 1 0]. The mask is arranged such that the length direction of the beam is along [1 1 0] orientation. The schematic diagram for the beam is shown in Fig. 1a. The length of the beam is designed as 400 μm, 500 μm, 600 μm, and 700 μm; the width is 100 μm; and the thickness is designed as 50 μm and 60 μm. The variation of all dimensions of the beams is found to be 1 – 2 μm. This dimensional variation may cause 14% variation in the stress and strain due to the derivation of bending stress σ ($\sigma = Mc/I$) by the area moment of inertia $I = bh^3/12$, where b and h are width and thickness of the beam respectively. The fabrication procedure is listed in Table 1. SiO_2 and Si_3N_4 thin films are deposited on the Si wafer in step one as protection from following KOH etching. Lithography process transfers geometry of cantilever beam from mask 1 to the front surface. Then reaction ion etching (RIE) removes part of Si_3N_4 layer where no photoresist protects for initial patterning. SiO_2 and Si_3N_4 layers patterned by mask 2 on back side surface are stripped off by RIE, followed by KOH anisotropic etching. Finally, RIE and inductive coupling plasma (ICP) are adopted to remove patterned SiO_2/Si_3N_4 layers and the silicon layer respectively and achieve a micro-cantilever beam. The fabricated beam is shown in Fig. 1b.

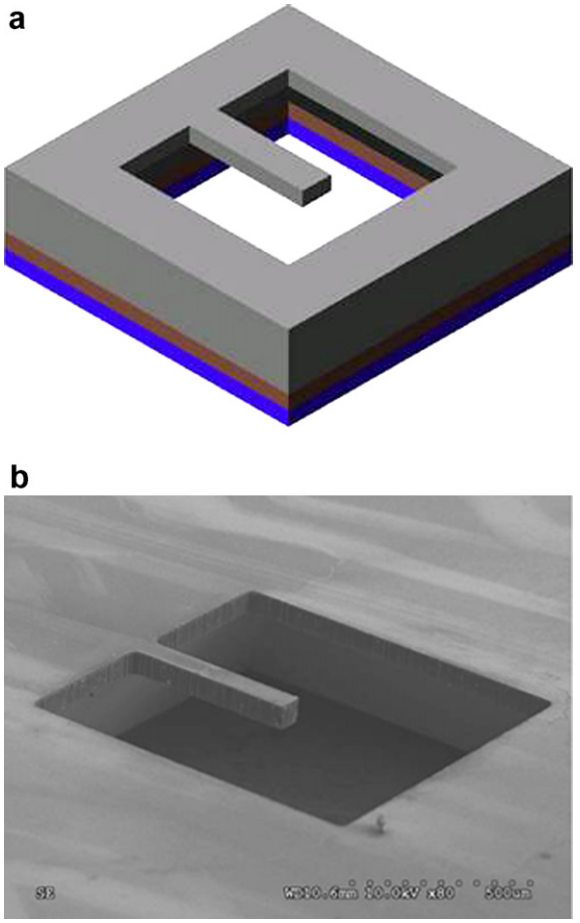

Fig. 1. (a) Schematic diagram and (b) SEM micrograph of the single crystal silicon (SCS) micro-cantilever beam.

2.2. Flexural testing

The fexural testing on the beam is conducted by the MTS Tytron 250 micro-force testing machine. The machine with testing set up is shown in Fig. 2a. The horizontal design of the machine and air bearing between actuator and frame at right-hand side enable the machine to overcome friction and achieve high precision. Therefore, the resolution of load and displacement can be up to 1 mN and 0.1 μm, respectively with the attachment of a 10-Newton (N) load cell and a precise displacement gauge. To conduct flexural test on a micro-cantilever beam, a special design of the fixture is adopted. As shown at left hand side in Fig. 2a, it is necessary to firmly clamp beams in wafer and precisely adjust the position of the beam. This was achieved by a precisely positioning x–y table sandwiched by two intermediate drilled plates, and an observing CCD system. The first intermediate plate fixes the x–y table on the frame of the testing machine. One side of the second intermediate plate attaches to the x–y table, and the other side has two small parallel rectangular plates with bolts that can press and fix the wafer on this side. In order to load on the beam, a tungsten micro-probe with a special design socket is firmly held on the load cell driven by the actuator of the machine to contact the beam.

The flexural test is conducted by first touching the probe on the free end of the cantilever beam as shown in Fig. 2b. Then the testing machine is

Table 1
Process steps for fabricating a single crystal silicon micro-cantilever beam

Step	Description
Starting material	4 in. silicon wafer
1. Deposition	Steam oxidizes SiO_2, and conduct LPCVD for Si_3N_4 on oxidized wafer as protection layers
2. Cleaning	Cleans deposited Si wafer by acetone
3. Photo-lithography 1	Spin coats AZ P4620 positive photoresist on deposited wafer
4. Heat treatment 1	Bakes photoresist at 90 °C
5. Lithography	Transfers cantilever beam pattern from mask 1 to wafer by exposing photoresist under ultraviolet light
6. Developing	Removes exposed photoresist by agent AZ 400 K
7. Heat treatment 2	Hardens unexposed photoresist
8. RIE etching	Selectively removes part of Si_3N_4 layer where no photoresist protects it for alignment and protection. The rest of the photoresist is removed
9. RIE back-side etching	Strips off SiO_2 and Si_3N_4 layers on back side patterned by mask 2 (a square)
10. KOH back-side etching	KOH etches Si from back side to a required thickness
11. Photo-lithography 2	Repeats steps 1–7 for patterning cantilever beam geometry
12. ICP etching	RIE etches patterned protection layers followed by penetrating Si layer by ICP etching
13. Finishing	Removes photoresist and beneath protection layers respectively by acetone and RIE

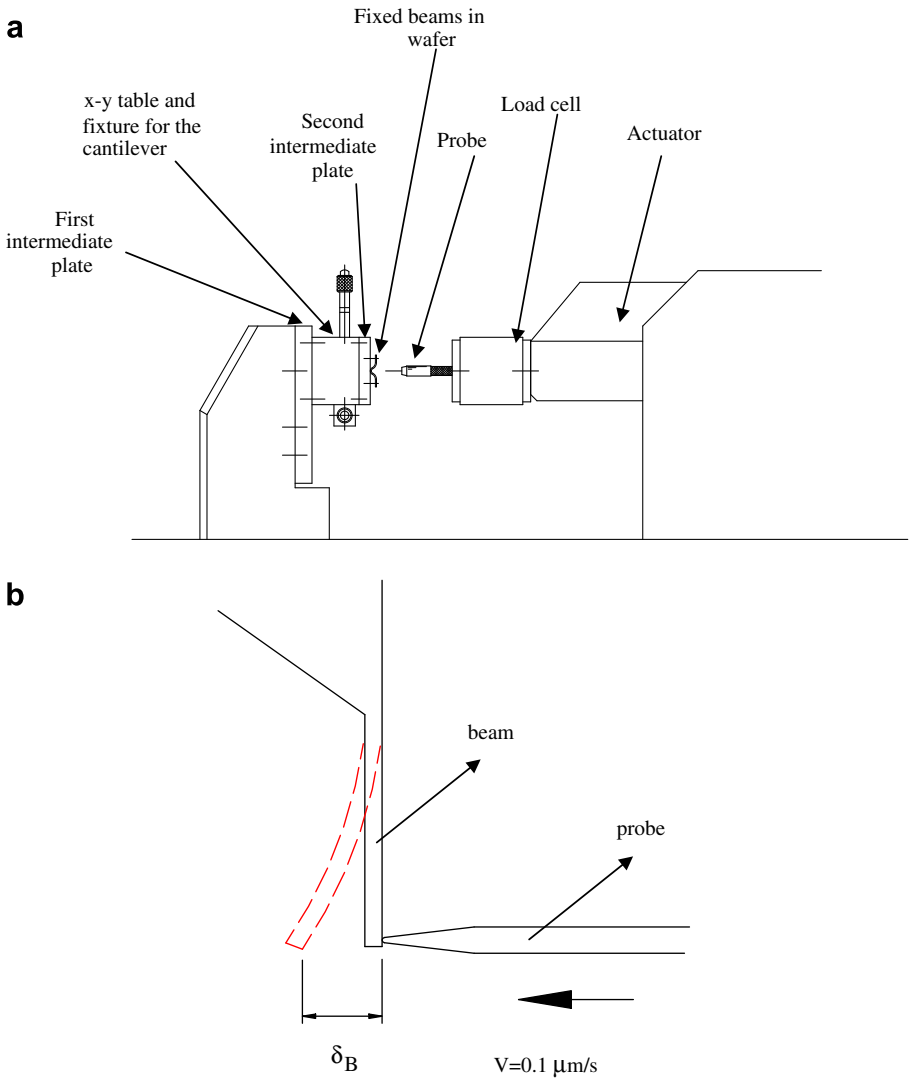

Fig. 2. Schematic diagram of (a) flexural testing of the SCS micro-cantilever beam and (b) close-up view of probe on the beam.

set up at a constant crosshead mode that the probe moves toward the beam at a constant rate of 0.1 μm/s. During the test, the force and displacement are recorded by the computer through the load cell and precise displacement gage in the machine in order to obtain flexural strength, failure strain, and Young's modulus. Five duplicate tests were conducted in order to obtain one valid data for stress, strain, or Young's modulus.

2.3. Characterization

In order to study the failure mechanism of bent beams, scanning electron microscope (SEM) is used to carefully observe failure modes of fractured beams with various dimensions. Surface roughness of mask patterned and KOH etched specimens is also measured by surface profiler to investigate its influence on strength.

3. Results and discussion

3.1. Stress–strain relationship

Fig. 3 shows flexural stress–strain relationships of beams with same width 100 μm, thickness 50 μm, lengths of 400 μm (Fig. 3a), and 700 μm (Fig. 3b); and thickness 60 μm, lengths of 400 μm (Fig. 3c), and 700 μm (Fig. 3d). Stresses and strains are derived from the forces and displacements as

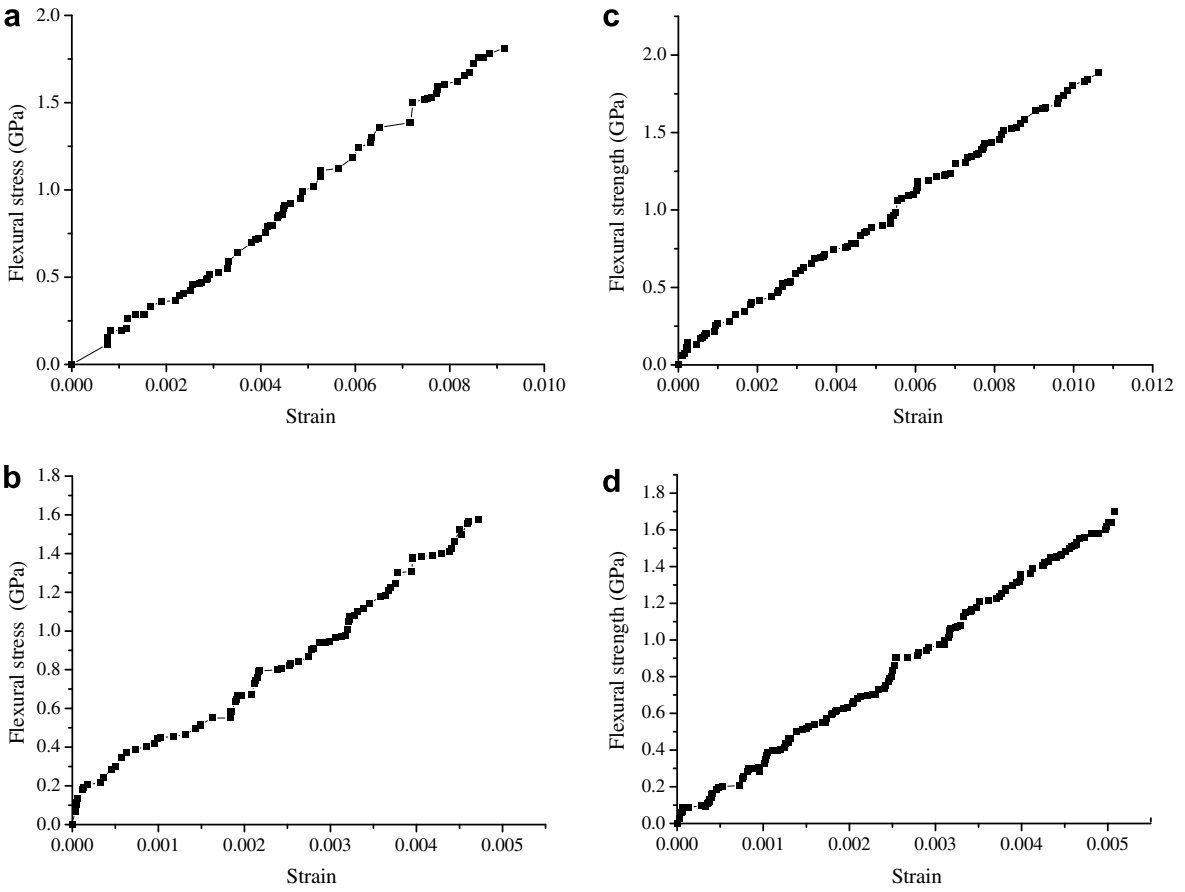

Fig. 3. Flexural stress–strain curves of beams with width 100 μm, thickness 50 μm, (a) length 400 μm and (b) length 700 μm; thickness 60 μm, (c) length 400 μm and (d) length 700 μm.

shown in Table 2 measured by micro-force testing machine. For 50 μm thick beams with various lengths, maximum forces decrease with increasing length and range from 0.189 N to 0.094 N, and maximum displacements range from 19.5 μm to 30.8 μm. While for 60 μm thick beams, maximum forces all increase and range from 0.284 N to 0.145 N but displacements decrease and range from 18.9 μm to 27.7 μm. As can be seen from Table 2 that error range of each data is larger than the resolution, this demonstrates the reliability of the stress–strain curve.

It can be cleared seen that the stress–strain relationship approximately follows a linear behavior, indicating that the brittle single crystal silicon (SCS) beam fails in an elastic manner subjected to bending. However, there is local zigzag in the stress–strain curve when the length of the beam increases. This could probably be caused either by a stick–slip mechanism at the probe–beam interface

Table 2
Maximum forces and displacements of beams with various dimensions subjected to bending

		Beam length (μm)			
		400	500	600	700
Maximum force (N)	Thickness 50 μm	0.189 ± 0.049	0.145 ± 0.044	0.117 ± 0.026	0.094 ± 0.029
	Thickness 60 μm	0.284 ± 0.038	0.217 ± 0.043	0.177 ± 0.021	0.145 ± 0.021
Maximum displacement (μm)	Thickness 50 μm	19.5 ± 7.8	20.8 ± 5.2	27.2 ± 6.3	30.8 ± 4.9
	Thickness 60 μm	18.9 ± 3.6	19.9 ± 2.5	23.9 ± 5.2	27.7 ± 3.6

or just by numerical noise, measurement noise that caused by the transduction of deformation and force into electrical voltage close to system resolution. Measurement errors caused by slippage of probe at the point of contact have been re-examined in stress–strain curves in Fig. 3. Compared with the linear trend of the whole stress–strain curve, the errors seem to be tolerable probably because the dimension of beam is in the micro-scale instead of nano-scale.

3.2. Young's modulus

Young's moduli for beams with various dimensions are obtained from the slope in their corresponding stress–strain curves. According to Fig. 3, Young's moduli are found in the range of 159.2–188.6 GPa for eight sets of beam dimensions, and are depicted individually in Table 3. The data show that Young's modulus is a fundamental material property which only depends on atomic bonding and crystal structure. The Young's modulus along [1 1 0] orientation 172 GPa is the average of the data shown in Table 3 and that this average has a standard deviation of 3.7 GPa. Given on the standard deviation the result is close to Brantly's result of 169 GPa [9]. This proves that the measuring method proposed in this work is valid. Young's moduli obtained by Brantly along three crystallographic directions [1 0 0], [1 1 0], and [1 1 1] are 130, 169, and 188 GPa respectively.

Table 3
Summary of Young's modulus

Young's modulus (GPa)	Length (μm)			
	400	500	600	700
Thickness 50 μm	165.3	172.8	166.3	188.6
Thickness 60 μm	164.0	159.2	177.0	183.9

3.3. Dimension effect

Table 4 shows flexural strengths and strains of beams with various dimensions derived from the data in Table 2. Although the variation of each data may be up to 20%, the trend of the strength or strain versus beam length (thickness) can be clear seen. As shown in Fig. 4, with constant beam width 100 μm and thickness 50 or 60 μm flexural strength of beam decreases as beam length increases from 400 to 700 μm. This result can be explained by the probability of existed flaws. During MEMS processing, the lithographically patterned flaws seem to inevitably be present in miniature structures such as microcantilever beams. For brittle materials the strength is governed by the maximum flaw size, typically at the surface. Simple statistical scaling arguments suggest that the probability of finding a flaw of a given size decreases with the volume (or area) of material under loading. It is the size and sharpness of the largest flaw that matter. Thus mechanical elements with small characteristic dimensions would be

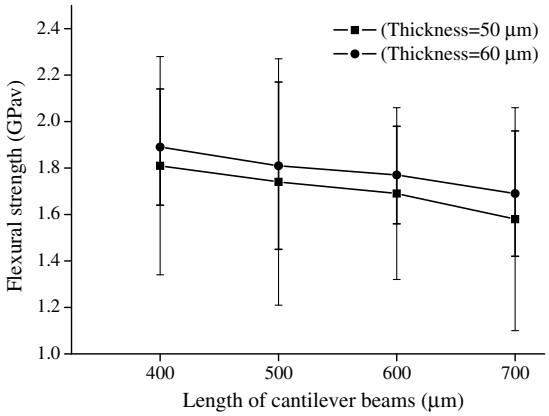

Fig. 4. Influence of beam length on flexural strength.

Table 4
Flexural strengths and strains of beams with various dimensions subjected to bending

		Beam length (μm)			
		400	500	600	700
Flexural strength (GPa)	Thickness 50 μm	1.81 ± 0.47	1.74 ± 0.53	1.69 ± 0.37	1.58 ± 0.48
	Thickness 60 μm	1.89 ± 0.25	1.81 ± 0.36	1.77 ± 0.21	1.69 ± 0.27
Flexural strain	Thickness 50 μm	$9.1 \times 10^{-3} \pm 3.6 \times 10^{-3}$	$6.2 \times 10^{-3} \pm 1.6 \times 10^{-3}$	$5.7 \times 10^{-3} \pm 1.3 \times 10^{-3}$	$4.7 \times 10^{-3} \pm 7.5 \times 10^{-4}$
	Thickness 60 μm	$1.1 \times 10^{-2} \pm 2.0 \times 10^{-3}$	$7.2 \times 10^{-3} \pm 9.0 \times 10^{-4}$	$6.0 \times 10^{-3} \pm 1.3 \times 10^{-3}$	$5.1 \times 10^{-3} \pm 6.6 \times 10^{-4}$

expected to be inherently stronger at small scales. The measured maximum displacement (δ) of the beam upon fracture in Table 2 can also be adopted to explain the phenomena. Once flaws exist at the fixed end of longer beams, the flaws seem to be more harmful to the beam because it fails with larger displacement, thus this leads to lower strength. This agrees with the statement that both geometry and stress distribution have to be considered to estimate the strength of MEMS since flaws are non-uniformly distributed [10].

For beams with same width and length, flexural strength increases with beam thickness as shown in Fig. 4. Flexural strength σ_f can be calculated by the following equation

$$\sigma_f = \frac{P}{t^2}\frac{6L}{b} \tag{1}$$

where P is the maximum applied loading upon fracture, b is the beam width, t the beam thickness, and L the beam length. When the beam thickness t decreases, the maximum applied loading P should decrease in proportion according to Eq. (1). However, in the thinner beam the maximum applied loading P is lower than expected due to edge surface roughness of 684 Å defined by the mask, i.e., thinner beam is more sensitive to surface roughness due to stress concentration. Minor evidence may be supported by the various surface roughness of 248.7 Å and 192.9 Å on 50 and 60 μm thickness beam surfaces, respectively, caused by KOH etching. The larger roughness on the 50 μm beam is probably due to the evolution of KOH etching solution in a longer period of etching time than that for the 60 μm beam. Unlike ceramics, there is no interior crack of SCS and surface flaws are strongly affect the brittle fracture of the SCS beams; therefore, this leads to lower strength in the thinner beam than in the thicker beam. This result infers that the influence of surface roughness on strength of beams is coupled with dimension.

This coupling effect can be further supported from the literature. According to Sundararajan et al. [10], a SCS beam with thickness 255 nm was fabricated by field-enhanced anodization using an AFM, and a bending strength of 18 GPa was measured. It is inferred that smaller surface roughness on this nano-scale beam surface has to be achieved by this specific processing route for enhancing the bending strength of the beams. Namazu [11] also concluded that beam strength from large to small in sequence is nano-beam, micro-beam, and milli-beam. It is suggested that various processing routes have to be adopted in above three categories of beams in order to obtain appropriate dimensions and surface roughness. However, in the same dimension range surface roughness caused by one processing route seems to be more effective on smaller specimen according to the results in this work.

The dimension of the beam also influences the flexural strain ε_f (Table 4). According to the following equation of flexural strain versus maximum displacement (δ)

$$\varepsilon_f = \frac{3t}{2L^2}\delta \tag{2}$$

where t is thickness of the beam, and L is length of the beam. Although maximum displacement increases with the beam length as shown in Table 2, flexural strain is inversely proportional to beam length L by a parabolic function as shown in Eq. (2). Thus, Fig. 5 depicts that flexural strain of the SCS micro-cantilever beam decreases with increasing beam length. The larger probability of defects exceeding a given size in the longer beam also inhibit the expected displacement of the beam, further leading to lower flexural strain in the beam. This also suggests that the ductility of the longer beam is lower than that of the shorter beam because ductility is proportional to flexural strain. The influence of thickness on flexural strain seems to reduce when the beam length increases, as can be seen by the closer trend of two curves in Fig. 5.

The above results show that our methodology using mechanical loading is able to test MEMS devices at higher force levels via micro-probes and generate reliable data for bending strength as well

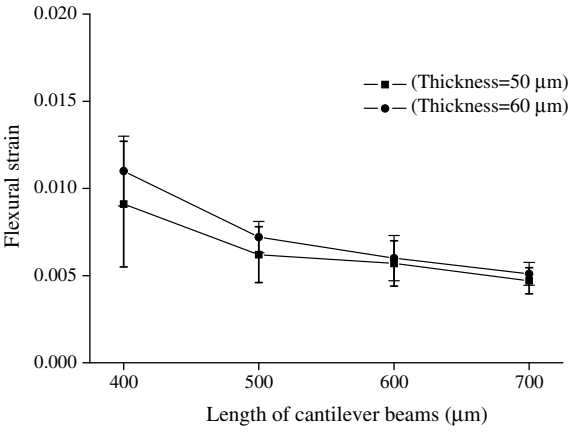

Fig. 5. Influence of beam length on failure strain.

as strain. These approaches are particularly necessary for the thicker structures realized by bulk micro-machining and LIGA processes. The device used in this work not only can apply for academic studies, but also is good for commercial applications. For example, bending strength is crucial for the design of a microaccelerometer. Through suitable design of the bending specimen with a "T" shape [12], torsional strength can be estimated on MEMS micromirrors using the results of the combined loading test. This testing result is essential for reliability for microswitches used in fiber optic networks in telecommunication as well as Texas Instruments Digital Micromirror Device (DMD). Using micro-force testing machine with designed fixtures, adhesion force of a poly(dimethylsiloxane) (PDMS) optical lens system can be evaluated. With a suitable design of optical grating on a PDMS chip, the chip can serve as an optical displacement sensor when properly calibrated by tension test on the machine.

3.4. Failure modes

The observation of bent fracture of the single crystal silicon (SCS) micro-cantilever beam can provide useful information of the failure modes and the failure mechanisms. The fracture surfaces of the SCS beams were observed using the scanning electron microscope (SEM) to provide this information as well as insight to various damage processes. Flexural failure modes of beams with various lengths, but same width 100 μm and thickness 50 μm, are shown in Fig. 6; while Fig. 7 depicts the failure modes of beams with different thickness of 60 μm.

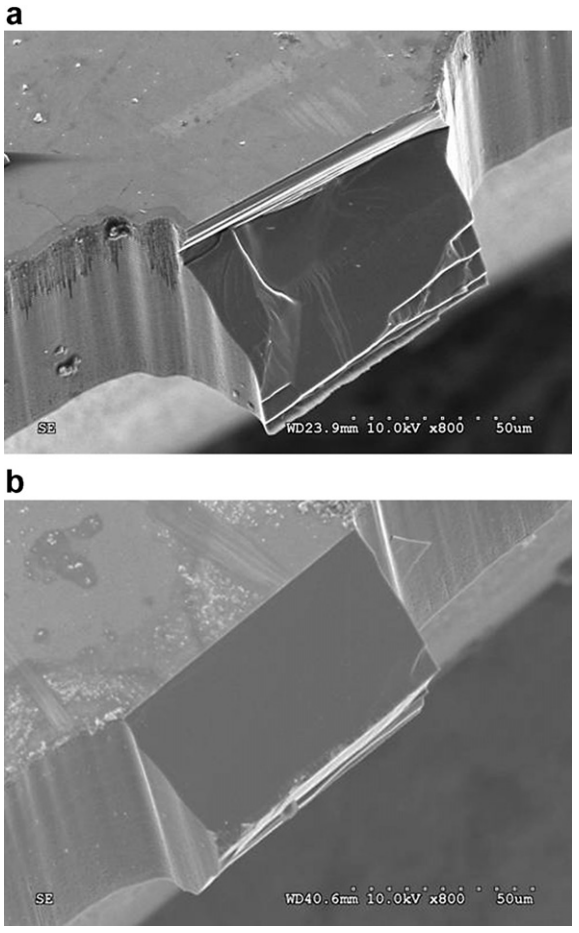

Fig. 6. Bending fracture of the micro-cantilever beam with width 100 μm, thickness 50 μm, and length of (a) 400 μm and (b) 700 μm.

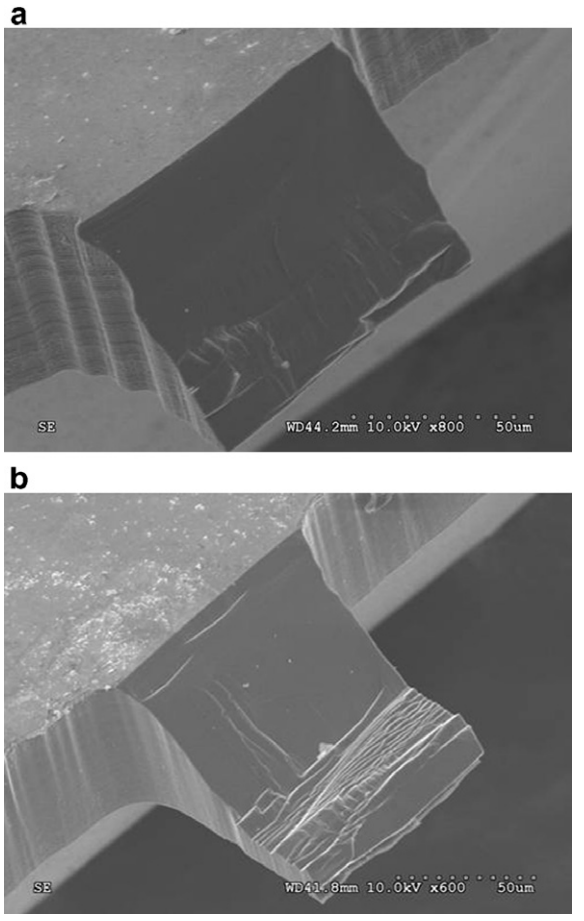

Fig. 7. Bending fracture of the micro-cantilever beam with width 100 μm, thickness 60 μm, and length of (a) 400 μm and (b) 700 μm.

Fig. 6a shows top view of bent fracture of the beam with beam length 400 μm. The dominant failure mode is cleavage initiated at, or near, the surface flaw along (1 1 1) plane. The cubic structure of SCS and top loading of the beam lead to fracture along this (1 1 1) plane having the lowest surface energy. The morphology shown here indicates that the bending crack initiates at fixed end of beam's top flat surface due to maximum tensile stress. On the broken surface, it can be clearly observed that high pitch striations lie approximately in the central area. It is noted that the probe transfers flexural loading normal to top surface of the beam, which results in tensile and compressive stresses at the upper and lower parts on broken surface, respectively, with striations as the border of the two opposite stresses. A zigzag pattern is found at the lower-right end of the fracture surface due to compressive stress. An undulated surface is also found at left end part of the broken surface probably due to

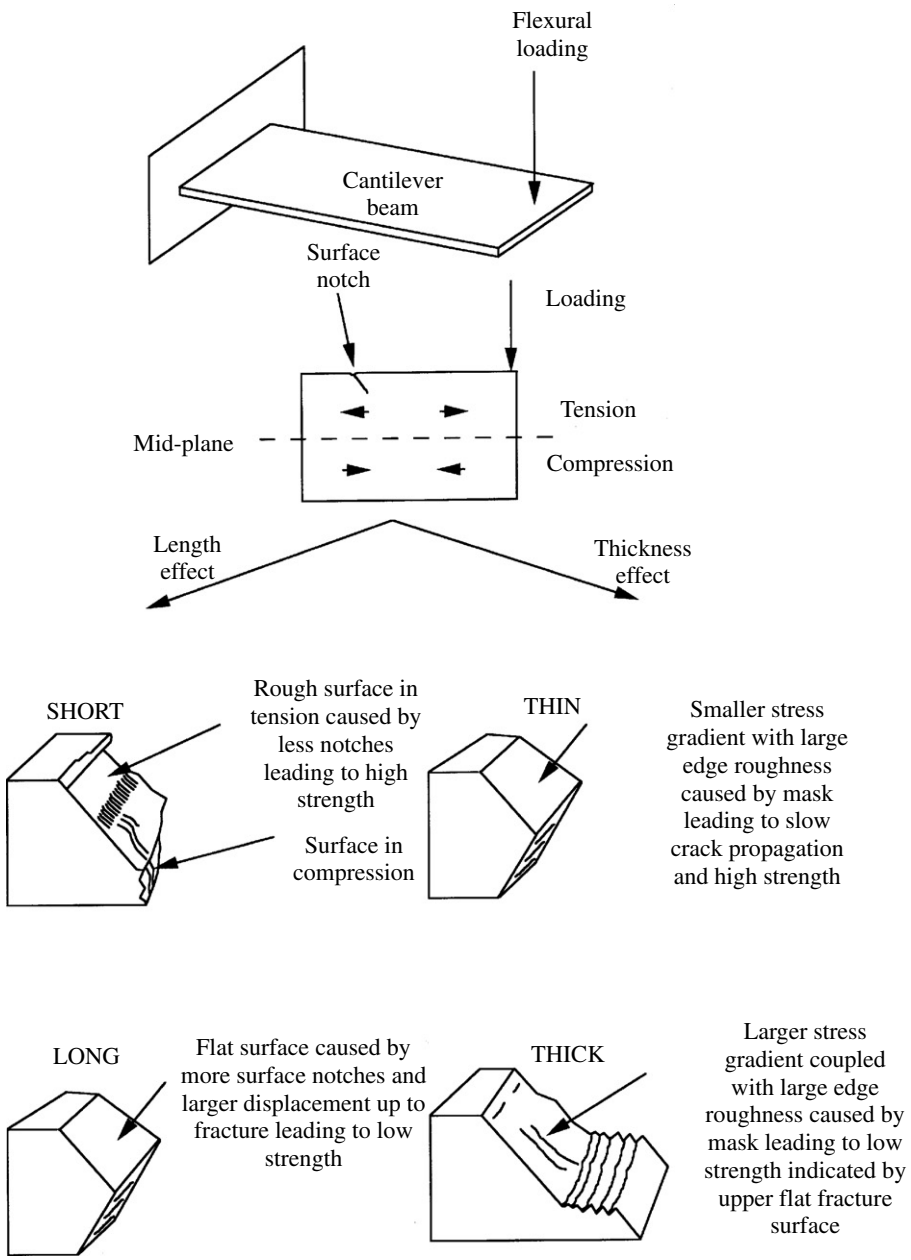

Fig. 8. Proposed failure mechanisms for various bent beams.

crack initiation from larger surface flaw. Jadaan [3] mentioned that the fracture of SCS could take place other than {1 1 1} planes with higher surface energies by right combination of stress magnitude and critical defects. This situation results in higher flexural strength. The micro-cantilever beams were ever side loaded to investigate this situation [13], and fracture initiated along (1 1 0) planes. However, the previous situation is not likely to occur in this work due to different loading conditions.

Fig. 6b depicts bent fracture of the beam with length of 700 μm. The failure mode is quite different from that of the 400 μm beam, which shows double fracture surfaces evenly along two {1 1 1} planes and upper {1 1 1} fracture plane is considerably flat. This observation is coincident with the result of lower strength for longer beam in that crack propagates easily along upper smooth {1 1 1} plane due to combination effect of surface flaws and larger displacement during testing.

Fig. 7a depicts bent fracture of the beam with length 400 μm and thickness 60 μm. A single fracture surface along (1 1 1) surface is observed. Compared to thinner beam of 50 μm in Fig. 6a, the upper surface of the thicker beam is more flat without the track of crack propagation caused by surface flaws. This infers that surface flaws could cause higher stress concentration in thinner beam and result in lower strength. Fig. 7b depicts bent fracture of the beam with length 700 μm. The morphology indicates that a larger flat (1 1 1) fracture plane is initiated from the top surface; however, this plane is not as flat as that in Fig. 6b. The crack propagation was slow down at the lower portion of broken surface subjected to compression, and changed as local peaks and valleys until final failure. This failure mode results in its lowest strength among beams with different lengths, but higher than the thinner beam with same length.

In Fig. 8, a summary of relationship between flexural strengths and failure modes is proposed. Basically there are three factors that influence the mode in a synergistic manner, including dimension of the beam, surface flaws, and loading condition. For short beam, the rough fracture surface caused by surface flaws indicates the difficulty of crack propagation and leads to higher strength. For longer beam, stress concentration at the fixed end of the beam caused by surface flaws is enhanced by large displacement, leading to lower strength. For thin beam subjected to bending, a large stress gradient occurs because stress distribution changes from tension to compression through a smaller thickness. This would lead to lower strength when coupled with large edge roughness caused by mask. For thick beam, the situation becomes less serious and results in higher strength.

4. Conclusions

The most significant advances in MEMS may occur by developing technologies to produce smaller devices with similar unit costs to those for existing microelectronics. To achieve this goal, the development of standard characterization techniques, particularly with regard to the mechanical properties, is very important if the full potential for paralleling the simulation-based design methodology achieved for IC devices is to be realized for MEMS. With a micro-probe, special designed fixtures, and a micro-force testing machine in this paper, complete mechanical properties and stress–strain curves of SCS micro-cantilever beams with various dimensions can be achieved. Furthermore, failure mechanisms are determined for various beams that are important to reliability of silicon. Several interesting findings are summarized as follows:

(1) For SCS beams with same width of 100 μm, length in the range of 400 – 700 μm, and thickness 50 – 60 μm, the flexural strength decreases with the increase of beam length, but increases with increasing thickness. The maximum strength is found to be 1.89 GPa for the beam with length 400 μm, thickness 60 μm, and width 100 μm.
(2) The influence of dimension on flexural strain of SCS beams has similar trend as that on flexural strength except that the thickness effect becomes negligible when beam length increases. The maximum flexural strain is 1.1×10^{-2} with the same dimension as the one having maximum strength, and flexural strain is proportional to ductility.
(3) Average Young's modulus along [1 1 0] orientation is found to be 172 GPa and irrelevant to beam dimension.
(4) For longer beam with lower strength, the major failure mode is double symmetric fracture surfaces along {1 1 1} planes with flat surface subjected to tension. Surface flaws and large displacement at the fixed end of beam result in the flat surface indicating the ease of crack propagation. On the other hand, thin

beam seems to be more sensitive to the same processing roughness than thicker beam within a similar dimensional range because larger stress gradient occurs in the thinner beam. This leads to lower strength in thinner beam.

(5) Using precise mechanical loading via micro-probes, the advantages of the proposed methodology is that it can simultaneously apply large force and displacement on MEMS devices, especially for thicker structures fabricated by bulk micro-machining and LIGA processes. This indicates that it can conduct testing on both force sensors and actuators such as microaccelerometers and micromirrors. This uniqueness may extent the methodology to evaluate more MEMS devices, for examples, optical lens and sensors, and simplify the processing route for some specimens tested by other means, such as electrostatic forces. The testing method can also be easily extended to nano-scale specimens by adding a force magnification lever mechanism. This work is now conducting in our laboratory.

Acknowledgment

Authors are grateful for financial support from National Science Council in Taiwan on this work under contract NSC 94-2212-E-035-005.

References

[1] A.B.O. Soboyejo, K.D. Bhalerao, W.O. Soboyejo, Reliability assessment of polysilicon MEMS structures under mechanical fatigue loading, J. Mater. Sci. 38 (2003) 4163–4167.

[2] W.N. Sharpe Jr., J. Bagdahn, K. Jackson, G. Coles, Tensile testing of MEMS materials-recent progress, J. Mater. Sci. 38 (2003) 4075–4079.

[3] O.M. Jadaan, N.N. Nemeth, J. Bagdahn, W.N. Sharpe Jr., Probabilistic Weibull behavior and mechanical properties of MEMS brittle materials, J. Mater. Sci. 38 (2003) 4087–4113.

[4] C.J. Wilson, A. Ormeggi, M. Narbutovskih, Fracture testing of silicon microcantilever beams, J. Appl. Phys. 79 (1995) 2386–2393.

[5] T. Y, L. Li, C-J Kim, Microscale material testing of single crystalline silicon: process effects on surface morphology and tensile strength, Sens. Actuators A: Phys 83 (2000) 172–178.

[6] C.J. Wilson, A.P. Beck, Facture testing of bulk silicon microcantilever beams subjected to a side load, J. MEMS 5 (1996) 142–150.

[7] O.M. Jadaan, N.N. Nemeth, J. Bagdahn, W.N. Sharpe Jr., Probabilistic Weibull behavior and mechanical properties of MEMS brittle materials, J. Mater. Sci. 38 (2003) 4087–4113.

[8] K.S. Chen, K.S. Ou, Equivalent strengths for reliability assessment of MEMS structures, Sens. Actuators A 112 (2004) 163–174.

[9] W.A. Brantly, Calculated elastic constants for stress problems associated with semiconductor devices, J. Appl. Phys. 44 (1972) 534–535.

[10] S. Sundararajan, B. Bhushan, T. Namazu, Y. Isono, Mechanical property measurements of nanoscale structures using an atomic force microscope, Ultramicroscopy 91 (2002) 111–118.

[11] T. Namazu, Y. Isono, T. Tanaka, Evaluation of size effect on mechanical properties of single crystal silicon by nanoscale bending test using AFM, J. Microelectromech. Syst. 9 (4) (2000) 450–459.

[12] S. Izumi, C.W. Ping, M. Yamaguchi, S. Sakai, Y. Ueda, A. Suzuki, Development of specimen and test method for strength analysis of MEMS micromirror, Eng. Fract. Mech. 72 (2005) 2672–2685.

[13] C.J. Wilson, A.P. Beck, Fracture testing of bulk silicon microcantilever beams subjected to a side load, J. Microelectromech. Syst. 5 (3) (1996) 142–150.